


# Measuring Thermal Emission Near Room Temperature Using Fourier-Transform Infrared Spectroscopy

Yuzhe Xiao,<sup>1</sup> Alireza Shahsafi,<sup>1</sup> Chenghao Wan,<sup>1,2</sup> Patrick J. Roney,<sup>1</sup> Graham Joe,<sup>1</sup> Zhaoning Yu,<sup>1,3</sup>  
Jad Salman,<sup>1</sup> and Mikhail A. Kats<sup>1,2,3,\*</sup>

<sup>1</sup>*Department of Electrical and Computer Engineering, University of Wisconsin-Madison, Madison, Wisconsin 53706, USA*

<sup>2</sup>*Department of Materials Science and Engineering, University of Wisconsin-Madison, Madison, Wisconsin 53706, USA*

<sup>3</sup>*Department of Physics, University of Wisconsin - Madison, Madison, Wisconsin 53706, USA*

 (Received 20 July 2018; revised manuscript received 9 October 2018; published 14 January 2019)

Accurate characterization of thermal emitters can be challenging due to the presence of background thermal emission from components of the experimental setup and the surrounding environment. This is especially true for an emitter operating close to room temperature. Here, we explore the characterization of near-room-temperature thermal emitters using Fourier-transform infrared (FTIR) spectroscopy. We find that the thermal background arising from optical components placed between the beam splitter and the detector in an FTIR spectrometer appears as a “negative” contribution to the Fourier-transformed signal, leading to errors in thermal-emission measurements near room temperature. Awareness of this contribution will help properly calibrate low-temperature thermal-emission measurements.

DOI: [10.1103/PhysRevApplied.11.014026](https://doi.org/10.1103/PhysRevApplied.11.014026)

## I. INTRODUCTION

Thermal emission is a fundamental physical process by which all objects at temperatures above 0 K emit light [1]. By analyzing thermally emitted light, information related to the emitter’s material properties [2] and temperature distribution [3] can be extracted. In the past decade, new developments in photonics and nanoscale fabrication have enabled research into engineered thermal emission [4,5] for applications that include passive radiative cooling [6], efficient incandescent light sources [7], and thermophotovoltaics [8]. Therefore, accurate experimental characterization of thermal emission has become increasingly important. Many thermal-emission measurements are performed via reflection and transmission measurements and the subsequent application of Kirchhoff’s law [9,10], which relates the emissivity of an object in thermal equilibrium to its absorptivity. However, this approach can be difficult for scattering [11] or highly absorbing samples [12]. Furthermore, in systems that are not in thermal equilibrium [13,14] or are not reciprocal [15,16], Kirchhoff’s law does not apply, and a direct measurement of the emitted light may be required. In the infrared region, where most thermal-emission measurements are performed, FTIR spectrometers are more commonly used compared to dispersive instruments due to

the so-called “multiplex advantage,” which describes the superior signal-to-noise ratio of FTIRs, especially at high resolution [17].

For a significant portion of thermal-emission research and development, such as for thermophotovoltaics, thermal-emission experiments are performed at high temperatures [10,18,19], such that the signal dominates over the thermal background emitted by components of the measurement instrument or the room that houses the experiment. However, recently, there has been growing interest in thermal emitters that operate at moderate temperatures [6,20,21], where direct-emission measurements can be challenging due to a low signal-to-noise ratio and a relatively large thermal background. Typically, interpreting FTIR-based thermal-emission measurements involves calibrating the FTIR response function and the background [22–24]. However, most studies that we have seen assume a response function that is independent of the sample temperature. This assumption turns out to potentially be problematic for cases where thermal emitters are close to room temperature.

In this work, we performed spectral measurements of near-room-temperature thermal emitters using an FTIR spectrometer and observed a background signal that sometimes appeared to be negative, and a sign inversion of the instrument response function when the sample temperature dropped below room temperature. We found that, in our instrument, these unexpected features arise from

\*mkats@wisc.edu

the background emission of the room-temperature optical components positioned between the interferometer and the detector. If such a background emission is present in an FTIR-based thermal-emission measurement apparatus, special care must be taken to extract quantitatively correct data.

## II. EXPERIMENTS

We used an FTIR spectrometer (Bruker VERTEX 70) to measure thermal-emission spectra from a laboratory blackbody (approximately 500- $\mu\text{m}$  tall vertically aligned carbon nanotube (CNT) forest [25]), as a function of temperature [Fig. 1(a)]. The sample is affixed on a temperature-controlled stage mounted inside the FTIR sample compartment, and was rotated by  $10^\circ$  with respect to the beam path to avoid multiple reflections between the sample and the interferometer (the reflections are not an issue for the highly absorbing blackbody,

but are for other samples). The thermal-emission signal from the sample was collected by a parabolic mirror, sent into a moving-mirror Michelson interferometer, and then detected by a liquid-nitrogen-cooled mercury-cadmium-telluride (MCT) detector. The collecting parabolic mirror has a small numerical aperture (approximately 0.05). In our setup, the beam path between the interferometer and detector includes several mirrors and apertures [“Optical components” in Fig. 1(a)].

In Fig. 1(b), we plot the measured emission spectra of the CNT blackbody from 10 °C to 30 °C. Note that the system was not purged, resulting in strong water and carbon dioxide absorption lines for wavelengths outside of the 8–14  $\mu\text{m}$  atmospheric transparency window. The measurement was performed with the temperature of the room housing the instrument ( $T_{\text{room}}$ ) set to 23 °C. As expected, the measured signal increases when the sample is heated above  $T_{\text{room}}$ . However, when the sample is cooled substantially below  $T_{\text{room}}$ , the measured signal also

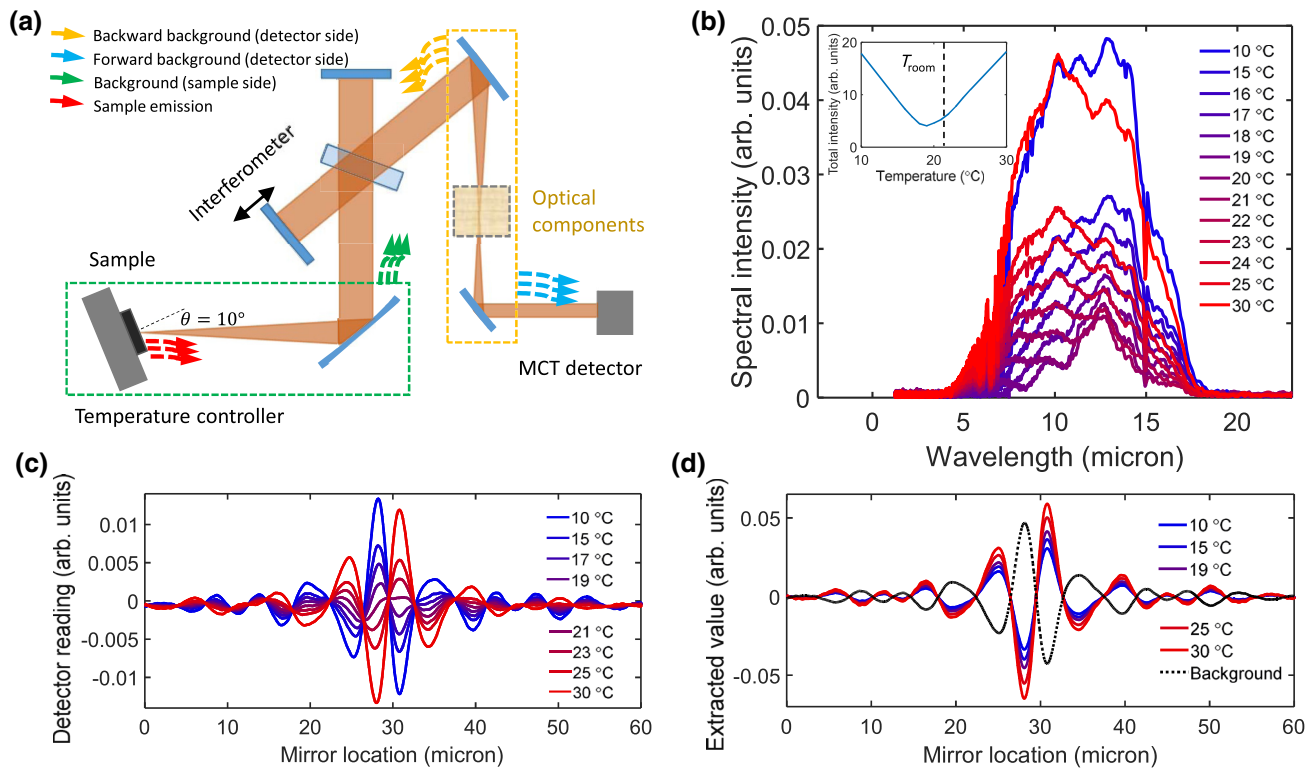


FIG. 1. (a) The optical path of our FTIR spectrometer. Light emitted from the sample (red arrows) is collected by a parabolic mirror, traverses the interferometer, passes through several optical components (mirrors and apertures), and is then sent to a liquid-nitrogen-cooled MCT detector. Most of the instrument components are at approximately room temperature, which results in several sources of background emission in both the forward (green and blue arrows) and backward (yellow arrows) directions. (b) Measured uncalibrated spectral intensity from the carbon nanotube (CNT) laboratory blackbody from 10 °C to 30 °C, which is minimized near 19 °C and increases when the sample is either heated or cooled. Inset: the integrated (but still uncalibrated) total spectral power over all wavelengths. The temperature of the room housing the experiment,  $T_{\text{room}}$ , is 23 °C. (c) Selected interferogram traces corresponding to the spectra in (b). The amplitude of the interferogram trace is minimized when the sample temperature is near 19 °C, and there is a  $\pi$  phase shift between the traces when the sample temperature is above (red lines) and below (blue) 19 °C. (d) Extracted contributions from the sample (solid lines) and the combined background (black dotted).

increases, appearing to contradict physical intuition and Planck’s law. The transition between these two distinct behaviors occurs when the sample temperature is around 19 °C. This unexpected experimental observation does not seem to have been previously discussed in the photonics and thermal-emitter-engineering literature, though it has been reported in the remote-sensing community [26].

In Fig. 1(c), we plot several of the experimental interferogram traces that are Fourier-transformed to obtain the spectra shown in Fig. 1(b). Note that parts of the interferogram can be negative because our detector is ac-coupled. We observe that the interferogram traces for temperatures above and below 19 °C are roughly out of phase. Like the resulting spectrum, the magnitude of the interferogram is minimized around 19 °C.

### III. INTERFEROGRAM ANALYSIS

In most FTIR spectrometers, including our own, all components except for the sample and the detector are kept at approximately room temperature. Therefore, the non-negligible thermal emission from the various components of the instrument and the surrounding environment (together they are the “background”) must be accounted for during data analysis. In particular, there can be background emission from components located both before and after the interferometer. The emission from components located before the interferometer [e.g., emission from the walls of the sample compartment that is reflected or scattered by the sample; green arrows in Fig. 1(a)] shares the same optical path as the sample emission: both are modulated via transmission through the interferometer and then received by the detector. This part of the background adds to the total detected signal. The forward-emitting background [blue arrows Fig. 1(a)] from components located after the interferometer is transmitted directly to the detector without modulation, and thus does not contribute to the detected signal. Finally, the backward-emitting background from components located between the interferometer and the detector [yellow arrows, Fig. 1(a)] is modulated via reflection from the interferometer and then received by the detector. As explained in the following, this contribution is apparently subtracted from the total detected signal.

To understand the origin of this “negative” background signal, it is helpful to separate the experimental interferogram,  $I(x, T)$ , into a sum of the temperature-dependent emission from the sample,  $I_S(x, T)$ , and a temperature-independent background,  $I_B(x)$ :

$$I(x, T) = I_S(x, T) + I_B(x). \quad (1)$$

In Eq. (1),  $x$  is the location of the moving mirror in the interferometer,  $T$  is the sample temperature, and  $I_B(x)$  represents the total background signal, which is due to all of the contributions indicated by the yellow, blue, and

green arrows in Fig. 1(a). Note that  $I_B$  can also become temperature dependent if the sample reflectivity is temperature dependent—via background emission reflected or scattered by the sample into the beam path—though this is not the case here. Using Eq. (1), these two components can be extracted from the experimental interferogram (more information in Sec. II of Supplemental Material [27]), and are plotted in Fig. 1(d). In our experiment, the amplitude of the sample interferogram increases monotonically with increasing sample temperature, and the background interferogram is out of phase with the sample interferogram (note that we are referring to the interferogram phase rather than the phase of the electromagnetic waves). Due to this  $\pi$  phase shift, the combined interferogram—and the resulting emission spectrum—is effectively representative of the difference between the two contributions rather than the sum. When the sample temperature is high, the sample emission dominates, and the total interferogram is close to that of the sample alone. Conversely, background emission dominates when the sample temperature is significantly below room temperature. The transition temperature at which the total interferogram is minimized is close to room temperature. Note that, naively, an interferogram is expected to be symmetric about the zero-path-difference point [28] but, in practice, interferometers can have path differences that change with frequency, leading to asymmetry [29].

To confirm that the negative background indeed comes from background emission of room-temperature components, we performed thermal-emission measurements at several different temperatures of the room housing the experiment. Increasing the room temperature should result in an increase of the magnitude of the background emission, and thus the temperature at which the measured integrated spectral power is minimized. The experimental results agree with this prediction (more information in Sec. III of Supplemental Material [27]).

### IV. ANALYSIS OF THE INTERFEROMETRIC PHASE

The  $\pi$  phase shift of the background interferogram arises from the reflection of the backward-emitting background radiation by the interferometer, in contrast to the forward-emitting radiation from the sample and background, which is modulated by the interferometer via transmission. The differences in the phase shifts imparted by Michelson interferometers in reflection and transmission modes were discussed in the early 1990s [30,31], and an explanation of this effect assuming a simple Fabry-Perot model for an FTIR beam splitter was given in Ref. [31]. However, we are unaware of general discussions on this topic that do not assume a specific type of beam splitter. Here, we provide a simple, general explanation for the  $\pi$

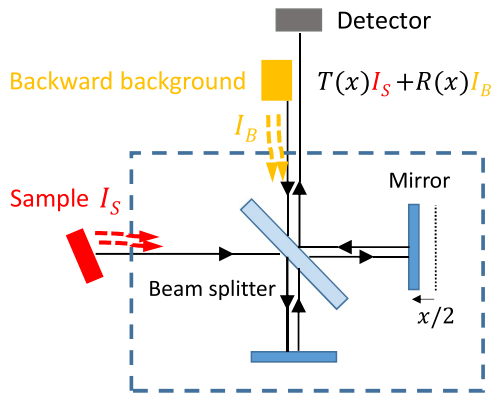


FIG. 2. Interaction of two thermal emitters (“Sample” and “Backward background”) with an interferometer. The sample emission is modulated via transmission through the interferometer, whereas the backward background is modulated via reflection. The signal received by the detector is the sum of the two contributions.

phase shift that is agnostic to the details of the interferometer except for the assumption that the beam splitter is not too lossy.

The interaction of a Michelson interferometer with two emitters (“Sample” and “Backward background”) is schematically shown in Fig. 2. As in the experiment, the sample is rotated with a non-zero angle to the interferometer path so that multiple reflections need not be considered. The propagation of light in the forward and backward directions through the interferometer can be defined by transmission and reflection coefficients. To simplify the analysis, we assume that the interferometer is lossless (i.e., no absorption or scattering at the beam splitter and mirrors) and reciprocal (i.e., the transmission is identical in both directions [32]). The reflection and transmission coefficients,  $R(x)$  and  $T(x)$ , respectively, depend on the position of the moving mirror,  $x$ . The sample emission,  $I_S$ , is transmitted through the interferometer and received by the detector, and the backward-emitting background,  $I_B$ , is reflected by the interferometer toward the detector. The total signal received by the detector is therefore:  $T(x)I_S + R(x)I_B$ . For a lossless interferometer [i.e.,  $T(x) + R(x) = 1$ ], the detected signal becomes

$$I(x) = T(x) \cdot (I_S - I_B) + I_B. \quad (2)$$

Note that in Eq. (2), the second term, “ $I_B$ ,” is not seen by an ac-coupled detector because it is independent of  $x$ . Therefore, the detected signal becomes  $T(x) \cdot (I_S - I_B)$ . Thus, when the sample emission is comparable to the background emission ( $I_S \approx I_B$ ), which can be the case for near-room-temperature samples, the total measured interferogram signal can be small [ $I(x) \approx 0$ ]. Although our analysis assumes a lossless interferometer, Eq. (2) is also a good approximation for an interferometer with

finite loss (i.e., if the beam splitter is partially absorbing), and explains the counterintuitive temperature-dependent interferogram traces in Fig. 1(c) and 1(d).

## V. IMPACT OF THE “NEGATIVE” BACKGROUND

For an FTIR spectrometer, the measured Fourier-transformed emission signal  $S_\alpha(\lambda, T)$  from a sample  $\alpha$  is often expressed as [22–24]

$$S_\alpha(\lambda, T) = \eta(\lambda)[\epsilon_\alpha(\lambda)I_{\text{BB}}(\lambda, T) + B_\alpha(\lambda)], \quad (3)$$

where  $\eta(\lambda)$ ,  $\epsilon_\alpha(\lambda)$ ,  $I_{\text{BB}}(\lambda, T)$ , and  $B_\alpha(\lambda)$  represent the system response, sample emissivity, blackbody radiation from Planck’s law [33], and the background emission, respectively. Note that the background can be sample-dependent; for example, there can be background thermal emission from the sample side reflected or scattered by the sample into the beam path. This analysis assumes a single combined background, which can arise from a combination of sources before and after the interferometer; knowledge of the precise breakdown of each contribution may not be necessary. From Eq. (3), the emissivity of sample  $\alpha$  can be obtained using a reference sample  $\beta$  with known emissivity  $\epsilon_\beta(\lambda)$  via

$$\epsilon_\alpha(\lambda) = \epsilon_\beta(\lambda) \frac{S_\alpha(\lambda, T_1) - S_\alpha(\lambda, T_2)}{S_\beta(\lambda, T_1) - S_\beta(\lambda, T_2)}. \quad (4)$$

Note that Eq. (4) assumes the sample emissivity does not change significantly with temperature, which is the case for most thermal emitters. To obtain the emissivity using Eq. (4), emission measurements at two different temperatures,  $T_1$  and  $T_2$ , can be used.

To illustrate the influence of this “negative” background on FTIR-based thermal-emission measurements, we measure thermal emission from a polished fused-silica wafer and a laboratory blackbody using the same setup, varying the temperature from 5 °C to 35 °C in steps of 1 °C (more information in Sec. IV of Supplemental Material [27]). No polarizer was used in this measurement. We selected  $T_1$  and  $T_2$  with a small interval of  $T_2 - T_1 = 5$  °C, and then extracted the emissivity of silica using Eq. (4).

In Fig. 3(a), we plot the experimental emissivity of the fused-silica wafer from 7 to 16  $\mu\text{m}$ , extracted using Eq. (4) and data from different five-degree temperature ranges, within an overall range from 10 °C to 25 °C. For reference, we calculate the emissivity using Kirchhoff’s law (green curve), using the optical properties of fused silica from variable-angle spectroscopic ellipsometry (VASE) and Fresnel coefficients (more information in Sec. V of Supplemental Material [27]). The emissivity value extracted using emission data from  $T_1 = 10$  °C and  $T_2 = 15$  °C (blue curve) has very large errors near 9 and 13  $\mu\text{m}$ . The value extracted using the emission data from

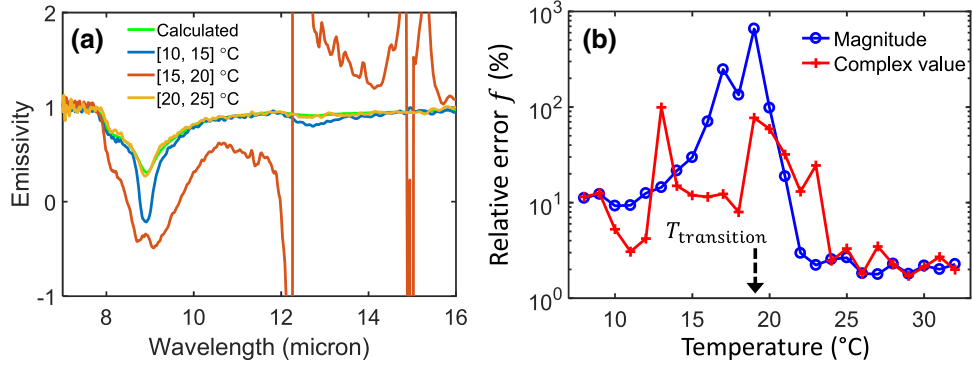


FIG. 3. (a) Measured polarization-averaged emissivity of a thick fused-silica sample at an angle of  $10^\circ$ , extracted from the magnitude of the measured spectrum (i.e., the magnitude of the Fourier transform of the interferogram), from different temperature ranges. The corresponding calculation based on optical constants from spectroscopic ellipsometry is shown in green. (b) Averaged relative error [Eq. (5)] in the extracted emissivity as a function of the central temperature at which the emission data was taken, using only the magnitude of the spectrum (blue) or the full complex value (red).

$T_1 = 15$  °C and  $T_2 = 20$  °C (red curve) has large errors at almost every wavelength, because this range includes the temperature at which the detected FTIR signal is minimized,  $T_{\text{transition}} \sim 18$  °C. As shown in Fig. 1(b), when the sample temperature crosses  $T_{\text{transition}}$ , the system response function  $\eta(\lambda)$  changes its sign: as the sample temperature is increased, the measured signal increases above  $T_{\text{transition}}$ , but decreases below  $T_{\text{transition}}$ . Clearly, Eq. (3) is no longer valid near  $T_{\text{transition}}$ . Therefore, one should always make sure  $T_1$  and  $T_2$  are both on the same side of  $T_{\text{transition}}$  when applying Eq. (4). As the data collection temperature range is increased above  $20$  °C (yellow curve), the measured emissivity becomes close to the calculated value (green curve).

To quantify this effect, we calculated the emissivity  $\epsilon_{\text{exp}}(\lambda, T)$  by gradually changing the central temperature  $T$  ( $T_1 = T - 2$  and  $T_2 = T + 2$ ), and obtained the relative error using

$$f(T) = \frac{1}{\lambda_2 - \lambda_1} \int_{\lambda_1}^{\lambda_2} \frac{\epsilon_{\text{exp}}(\lambda, T) - \epsilon_c(\lambda)}{\epsilon_c(\lambda)} d\lambda, \quad (5)$$

where  $\epsilon_c(\lambda)$  is the calculated emissivity [green curve, Fig. 3(a)], which we assume to be exact. The relative error  $f$  is plotted in Fig. 3(b) for different central  $T$ , with  $\lambda_1$  and  $\lambda_2$  chosen to be 7 and  $16 \mu\text{m}$ , respectively. In the same figure,  $T_{\text{transition}}$ , the temperature at which the measured emission signal is minimized, is identified. The large error near  $T_{\text{transition}}$  is the result of the change of the system response of the FTIR spectrometer;  $f$  decreases at both lower and higher temperatures. An asymmetry of  $f$  with respect to  $T_{\text{transition}}$  is observed, which is related to the fact that the negative background does not fully cancel out the sample emission at  $T_{\text{transition}}$ , and the measured signal is not minimized at every wavelength at  $T_{\text{transition}}$ .

An alternative calibration method that was proposed in Ref. [23] uses the full complex measured spectrum (i.e.,

the Fourier transform of the interferogram) instead of using only the magnitude, as we did in Eqs. (3) and (4). This complex spectrum can be expressed as

$$\tilde{S}_\alpha(\lambda, T) = \eta(\lambda) [\epsilon_\alpha(\lambda) I_{\text{BB}}(\lambda, T) + B_\alpha(\lambda) e^{i\vartheta_{0,\alpha}(\lambda)}] e^{i\vartheta_\alpha(\lambda)}, \quad (6)$$

where  $\vartheta_{0,\alpha}$  is the background phase and  $\vartheta_\alpha$  is the instrument-response phase, both for sample  $\alpha$ . Then, the emissivity can be extracted using

$$\epsilon_\alpha(\lambda) = \epsilon_\beta(\lambda) \left| \frac{\tilde{S}_\alpha(\lambda, T_1) - \tilde{S}_\alpha(\lambda, T_2)}{\tilde{S}_\beta(\lambda, T_1) - \tilde{S}_\beta(\lambda, T_2)} \right|. \quad (7)$$

The calibration error using Eq. (7) is also plotted in Fig. 3(b). Compared to the use of Eq. (4), the error is reduced close to  $T_{\text{transition}}$ , where it is nevertheless very large using either method. For sample temperatures significantly above  $T_{\text{transition}}$ , Eq. (4) seems to be more robust.

Since the thermally radiated power from an emitter depends on its emissivity, the value of  $T_{\text{transition}}$  depends on the emissivity of both the sample and the background. More specifically,  $T_{\text{transition}}$  is expected to increase for an emitter with a lower emissivity. Therefore, such a negative background could have an impact on even a relatively high-temperature thermal-emission measurement when the sample has a low emissivity.

## VI. FURTHER DISCUSSION AND CONCLUSION

In principle, if one were to place the detector immediately after the interferometer, any backward-propagating background emission should be negligible. In practice, FTIR systems are often multifunctional, e.g., set up for some combination of transmission, reflection, emission, and other measurements, possibly with removable or fixed accessories such as microscopes and custom stages. For

example, our system has a number of emitting components that contribute to the background, including several aluminum mirrors, a prism for coupling of a laser pump, and apertures that restrict the area of detection on the sample. We believe that many FTIR-based systems have emitting components that may be impractical to remove and that must be accounted for following the approach outlined above. Alternatively, a room-temperature detector can be utilized, which would then be in equilibrium with all of the background sources. This approach, however, can result in low signal-to-noise ratios [34], and requires that the detector temperature is identical to that of the background sources.

If the emissivity of the sample does not change with temperature, one can avoid the impact of the negative background by measuring its thermal emission at a higher temperature and obtain accurate results using Eqs. (3) and (4). However, there are some cases where one must perform low-temperature measurements (e.g., the experiments in refs. [6,20,21]). If the target thermal-emission temperature is close to  $T_{\text{transition}}$ , one solution is to decrease the ambient temperature to a lower  $T_{\text{transition}}$ .

Further complications occur for thermal emitters near room temperature whose emissivity is temperature-dependent (e.g., those in Refs. [35–37]). In this case, one needs not only to decrease the ambient temperature, but also to choose  $T_1$  and  $T_2$  that are close enough to each other such that the emissivity is not very different at the two temperatures; this approach can result in low signal-to-noise ratios. Finally, for nonequilibrium or non-reciprocal systems where Kirchhoff's law does not apply, the background must be fully calibrated to obtain the actual thermal-emission signal.

We note that the peculiarities described in this manuscript can be avoided by using dispersive spectrometers. However, the “multiplex advantage” and other features of FTIRs make them otherwise ideal for various mid-infrared measurements, especially for situations with weak signals (e.g., low-temperature thermal emission) or narrowband features (see the discussion on narrowband emitters in Ref. [5]).

To summarize, in this work we observed counterintuitive phenomena when performing near-room-temperature thermal-emission measurements using an FTIR spectrometer, i.e., an apparent “negative” background signal and a sign inversion of the system response function. We found that these features arise from the background emission of optical components positioned between the interferometer and the detector. Similar behavior has been previously discussed in remote-sensing literature, but not in the nanophotonics and thermal-emission-engineering communities. We expect these and related issues to be significant in different kinds of FTIR systems, and have provided suggestions and guidance on how to perform and interpret low-temperature thermal-emission measurements.

## ACKNOWLEDGMENTS

The authors acknowledge discussions with Romain Blanchard from Pendar Technologies and Daniel Wasserman from University of Texas - Austin. This work is supported by the Office of Naval Research (Grant No. N00014-16-1-2556) and the Department of Energy (Grant No. DE-NE0008680).

- 
- [1] L. Landau and E. Lifshitz, *Statistical Physics* (Oxford, Pergamon Press, 1980).
  - [2] C. Rao, *Chemical Applications of Infrared Spectroscopy* (Academic Press, New York, 1963).
  - [3] M. D. Smith, J. C. Pearl, B. J. Conrath, and P. R. Christensen, Thermal Emission Spectrometer results: Mars atmospheric thermal structure and aerosol distribution, *J. Geophys. Res. Planets* **106**, E10 (2001).
  - [4] W. Li and S. Fan, Nanophotonic control of thermal radiation for energy applications, *Opt. Express* **26**, 12 (2018).
  - [5] D. G. Baranov, Y. Xiao, I. A. Nechepurenko, A. Krasnok, A. Alù, and M. A. Kats, Nanophotonic engineering of active and functional thermal emitters, arXiv:1806.03372 (2018).
  - [6] A. P. Raman, M. A. Anoma, L. Zhu, E. Rephaeli, and S. Fan, Passive radiative cooling below ambient air temperature under direct sunlight, *Nature* **515**, 7528 (2014).
  - [7] O. Ilic, P. Bermel, G. Chen, J. D. Joannopoulos, I. Celanovic, and M. Soljačić, Tailoring high-temperature radiation and the resurrection of the incandescent source, *Nat. Nanotechnol.* **11**, 320 (2016).
  - [8] J. A. Duffie and W. A. Beckman, *Solar Engineering of Thermal Processes* (Wiley, Hoboken, 2013).
  - [9] I. Celanovic, N. Jovanovic, and J. Kassakian, Two-dimensional tungsten photonic crystals as selective thermal emitters, *Appl. Phys. Lett.* **92**, 19 (2008).
  - [10] P. N. Dyachenko, S. Molesky, A. Y. Petrov, M. Störmer, T. Krekeler, S. Lang, M. Ritter, Z. Jacob, and M. Eich, Controlling thermal emission with refractory epsilon-near-zero metamaterials via topological transitions, *Nat. Commun.* **7**, 11809 (2016).
  - [11] J. E. Moersch and P. R. Christensen, Thermal emission from particulate surfaces: A comparison of scattering models with measured spectra, *J. Geophys. Res.* **100**, E4 (1995).
  - [12] I. Šimon, Spectroscopy in infrared by reflection and its use for highly absorbing substances, *J. Opt. Soc. Am.* **41**, 5 (1951).
  - [13] L. Tsang, E. Njoku, and J. A. Kong, Microwave thermal emission from a stratified medium with nonuniform temperature distribution, *J. Appl. Phys.* **46**, 12 (1975).
  - [14] C. H. Lui, K. F. Mak, J. Shan, and T. F. Heinz, Ultrafast Photoluminescence from Graphene, *Phys. Rev. Lett.* **105**, 12 (2010).
  - [15] L. Zhu and S. Fan, Near-complete violation of detailed balance in thermal radiation, *Phys. Rev. B* **90**, 22 (2014).
  - [16] Y. Hadad, J. C. Soric, and A. Alu, Breaking temporal symmetries for emission and absorption, *Proc. Natl. Acad. Sci.* **113**, 13 (2016).

- [17] W. D. Perkins, Fourier transform infrared spectroscopy: Part II. Advantages of FT-IR., *J. Chem. Educ.* **64**, A269 (1987).
- [18] Y. X. Yeng, M. Ghebrehbrhan, P. Bermel, W. R. Chan, J. D. Joannopoulos, M. Soljačić, and I. Celanovic, Enabling high-temperature nanophotonics for energy applications, *Proc. Natl. Acad. Sci. USA* **109**, 7 (2012).
- [19] X. Liu and W. J. Padilla, Thermochromic infrared metamaterials, *Adv. Mater.* **28**, 5 (2016).
- [20] X. Liu and W. J. Padilla, Reconfigurable room temperature metamaterial infrared emitter, *Optica* **4**, 4 (2017).
- [21] M. Zhou, H. Song, X. Xu, A. Shahsafi, Z. Xia, Z. Ma, M. A. Kats, J. Zhu, B. S. Ooi, Q. Gan, and Z. Yu, Accelerating vapor condensation with daytime radiative cooling, arXiv:1804.10736 (2018).
- [22] H. E. Revercomb, H. Buijs, H. B. Howell, D. D. LaPorte, W. L. Smith, and L. A. Sromovsky, Radiometric calibration of IR Fourier transform spectrometers: Solution to a problem with the High-Resolution Interferometer Sounder, *Appl. Opt.* **27**, 15 (1988).
- [23] E. Lindermeir, P. Haschberger, V. Tank, and H. Dietl, Calibration of a Fourier transform spectrometer using three blackbody sources, *Appl. Opt.* **31**, 22 (1992).
- [24] S. Clausen, A. Morgenstjerne, and O. Rathmann, Measurement of surface temperature and emissivity by a multitemperature method for Fourier-transform infrared spectrometers, *Appl. Opt.* **35**, 5683 (1996).
- [25] K. Mizuno, J. Ishii, H. Kishida, Y. Hayamizu, S. Yasuda, D. N. Futaba, M. Yumura, and K. Hata, A black body absorber from vertically aligned single-walled carbon nanotubes, *Proc. Natl. Acad. Sci. USA* **106**, 15 (2009).
- [26] A. Shimota, H. Kobayashi, and S. Kadokura, Radiometric calibration for the airborne interferometric monitor for greenhouse gases simulator, *Appl. Opt.* **38**, 3 (1999).
- [27] See Supplemental Material at <http://link.aps.org/supplemental/10.1103/PhysRevApplied.11.014026>. Section 1 shows the calibration of the FTIR system response function. Section 2 shows the process of extracting signal and background interferograms. Section 3 shows emission measurements with different ambient temperatures. Section 4 shows emission data for calibrating the emissivity of the fused silica wafer. Section 5 shows the emissivity of fused silica wafer from ellipsometry.
- [28] P. R. Griffiths and J. A. De Haseth, *Fourier Transform Infrared Spectrometry* (Wiley, Hoboken, 2007).
- [29] M. L. Forman, W. H. Steel, and G. A. Vanasse, Correction of asymmetric interferograms obtained in fourier spectroscopy, *J. Opt. Soc. Am.* **56**, 1 (1966).
- [30] C. Weddigen, C. E. Blom, and M. Höpfner, Phase corrections for the emission sounder MIPAS-FT, *Appl. Opt.* **32**, 4586 (1993).
- [31] J. M. Thériault, Beam splitter layer emission in Fourier-transform infrared interferometers, *Appl. Opt.* **37**, 36 (1998).
- [32] R. J. Potton, Reciprocity in optics, *Rep. Prog. Phys.* **67**, 5 (2004).
- [33] T. H. Boyer, Derivation of the blackbody radiation spectrum without quantum assumptions, *Phys. Rev.* **182**, 5 (1969).
- [34] A. Rogalski, Infrared detectors: An overview, *Infrared Phys. Technol.* **43**, 3 (2002).
- [35] M. A. Kats, R. Blanchard, S. Zhang, P. Genevet, C. Ko, S. Ramanathan, and F. Capasso, Vanadium Dioxide as a Natural Disordered Metamaterial: Perfect Thermal Emission and Large Broadband Negative Differential Thermal Emittance, *Phys. Rev. X* **3**, 4 (2013).
- [36] D. M. Bierman, A. Lenert, M. A. Kats, Y. Zhou, S. Zhang, M. D. L. Ossa, S. Ramanathan, F. Capasso, and E. N. Wang, Radiative thermal runaway due to negative differential thermal emission across a solid-solid phase transition, arXiv:1801.00376 (2017).
- [37] P. J. Roney, A. Shahsafi, Z. Zhang, Y. Zhou, C. Wan, R. Wambold, J. Salman, S. Ramanathan, and M. A. Kats, in *Conference on Lasers and Electro-Optics*, FM4G.2 (2017).